We appreciate the reviewer for the useful comments. In the following, original reviewer comments are shown in black, our point-by-point responses are shown in blue, and updates on the manuscript are shown in blue and highlighted in yellow.

Reviewer Comments to Author:

Reviewer: 2

In their manuscript **"Size-resolved isotope analysis reveals anthropogenic reactive nitrogen transport and transformation in Taiwan mountain forests"**, authors conducted size-resolved isotope analysis of aerosol sampled at a mountain forest in Xitou, Taiwan to reveal sources and processes. The study is on a topic of relevance and general interest to the readers of ACP. Methodologically, studying reactive nitrogen species with isotopic techniques and source attribution modeling is not new. I am mostly concerned with the short period of sampling (8 days, 2 filter samples per day) and the lack of gas-phase nitrogen-containing species measurement, which makes it hard to form conclusive sources and formation pathways identification. Yet the data in the region of study during a prolonged fog is valuable, and the analyses were carried out comprehensively and rigorously. I am recommending a minor revision with detailed comments listed below.

Specific comments:

R2C1: In Introduction, Line 66-81, the scientific significance of the study is not well explained. It is stated that "relatively little is known about the sources and atmospheric processing of Nr in East Asian mountain forests", yet the authors later referred to Chen, T. Y. et al. (2022) that used the similar methodology (isotope signatures) at the same location. I'd love to see the authors further highlight the uniqueness of the location; for example, is Xitou a representative mountain forest area for East Asian, or at least for Taiwan (meteorologically wise, BVOC profile wise, urban-forest mixing wise)? Is Xitou known for abundant nitrogen-containing particles, mass concentration wise or fractional wise? Moreover, more information should be added to highlight the importance of aerosol chemistry under fog conditions (and summarize the current knowns and unknowns on aqueous phase processing etc.), followed by how your size-dependent isotopic approach could improve such understanding (see comment#5). This will enhance the scientific uniqueness of your study and can actually distinguish it from the previous one.

Response: We appreciate the reviewer for raising this point. Xitou is representing a mountain forest environment in Taiwan and East Asia, which is affected by local emissions and regional pollution transport by mountain-valley circulation and complex diurnal and seasonal variations in mixing layer heights. This part, as well as the Nr concentrations and the importance of aerosol chemistry under fog conditions, were updated in the revised manuscript in the introduction section (Lines 73−85) as follows:

> (Lines 73−85) "Xitou, a representative cloud forest in central Taiwan, serves as an ideal natural laboratory to address these gaps. Situated in a valley oriented toward urban regions, the site experiences predictable valley-mountain breeze circulations that transport anthropogenic plumes into a biogenic-rich environment where Nr accounts for

13−23% of PM_{10} mass (Chen et al., 2021). This mixing vessel is characterized by frequent fog and persistent humidity, with a mean relative humidity (RH) above 80%. Fog droplets serve as a reactive aqueous medium, facilitating the dissolution of Nr species and accelerating secondary aerosol formation through aqueous-phase oxidation, thereby modifying aerosol hygroscopicity and chemical aging (Ervens, 2015). Specifically, aqueous-phase nitrate formation during fog proceeds via oxidation of NO_2 by ·OH radicals and heterogeneous hydrolysis of N_2O_5 on fog droplet surfaces. Furthermore, NO_2 disproportionation represents an additional pathway, a process enhanced by the larger radii of fog droplets compared to aerosol particles (Zhang et al., 2022; Lin et al., 2026; Yu et al., 2023). In addition, recent field research has demonstrated efficient nitrate formation during fog occurs mainly on fog interstitial aerosols through NO_2 and N_2O_5 hydrolysis, highlighting the importance of size-resolved characterization of aerosols under fog conditions (Xu et al., 2024). ”

R2C2: In Methods, Line 90, please justify your choice of the sampling period. Is April meteorologically favorable for foggy conditions or prone to higher ambient aerosol loadings or what? Is the week-long measurement representative enough for reaching your conclusions (e.g. those around Line 422)?

Response: We thank the reviewer for raising this point. We have added a justification for the choice of sampling period in the Methods section. The rationale addresses two aspects: the meteorological favorability for fog occurrence at Xitou in April, and the representativeness of the spring season in terms of aerosol loading and long-range transport influence.

- Fog conditions at Xitou in spring: Xitou is a mid-elevation cloud forest site in central Taiwan, situated in a mountainous subtropical island where forests cover more than 50% of the land area, and many highland sites experience over 100 fog days per year. Fog occurrence at Xitou is documented: Liang et al. (2009) reported 320 foggy days (visibility < 1000 m) at the site between April 2005 and March 2006, with the highest fog frequency concentrated between March and July (153 foggy days). Notably, the mean daily fog duration peaked in April at approximately 18.4 hours per day, making it the month with the most sustained fog cover within the year. Another study by Wey et al. (2011) also reported fog occurrence in April (14 foggy days; ~9 hours per day on average), though with lower frequency, likely reflecting interannual variability. Our own cloud ceilometer data collected at Xitou from 2017 to 2020 further corroborates that fog events occur frequently during spring (February–May, see Fig. R1 below). We therefore selected an April sampling window to maximize the likelihood of capturing fog processing of aerosols. It is also worth noting that while summer and winter have received more research attention at Xitou, spring, as a transitional season, is comparatively understudied, making our April dataset a useful contribution to the seasonal characterization of this site.
- Aerosol loading and long-range transport in spring: Beyond fog meteorology, April falls within a period of elevated aerosol loading in Taiwan. Ambient PM_{10} and $PM_{2.5}$ concentrations in Taiwan typically reach their seasonal maxima in winter and remain comparably elevated through spring, before declining to their minima in summer. This elevated loading is in part driven by long-range transport: Taiwan is situated at the junction

of the East and South China Seas in the northwestern Pacific, flanked by the Chinese mainland to the northwest, Japan to the northeast, and the Philippines to the south. During winter and spring, anticyclonic systems originating from the Mongolian Plateau traverse the industrial corridors and megacity regions of eastern China, potentially entraining mineral dust and anthropogenic pollutants that are subsequently transported to Taiwan. In addition, biomass burning emissions from Southeast Asia can influence aerosol composition in the region during spring. Sampling in April thus captures a period of active long-range pollutant influence, providing an opportunity to examine how transported nitrogen species interact with local fog processing and gas–particle partitioning at the mountain site.

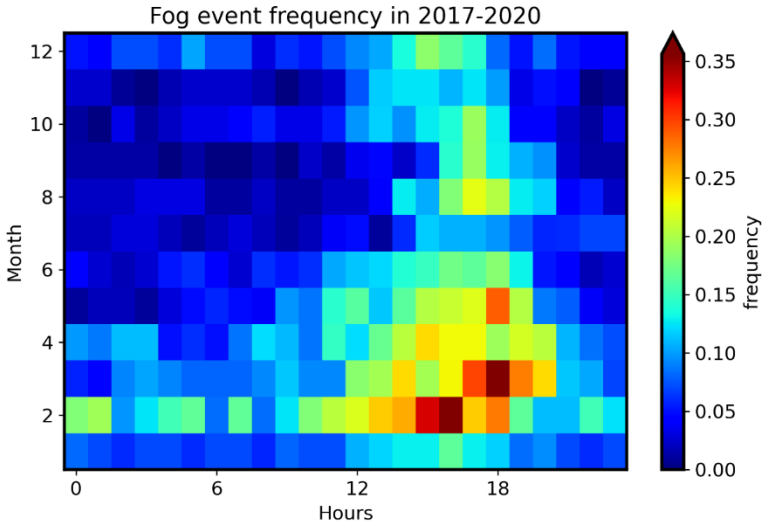

Figure R1. Monthly and diurnal distribution of fog event frequency at Xitou derived from ceilometer measurements during 2017–2020 (unpublished data, courtesy of co-authors).

On the representativeness of a week-long campaign, we acknowledge that a single week of observations carries inherent limitations for broader generalization. However, intensive short-term campaigns are a well-established approach in aerosol isotope studies, where the analytical demands of size-segregated impactor sampling and isotope ratio measurements preclude continuous year-round collection. The conclusions drawn around Line 422 are framed in terms of the processes observed during the campaign (e.g., fog aqueous-phase processing, transport signatures) rather than as climatological statements. We have clarified this point in the revised manuscript in the method section (Lines 97−99), section 3.4.2 (Lines 428−430), and the conclusions section (Lines 479−481) as follows:

> (Lines 97−99) “April represents the spring transition in Taiwan, a period characterized by frequent fog at Xitou, and a shift in aerosol loading from wintertime maxima to summertime minima.”
>
> (Lines 428−430) “[…] However, given the limited number of sampling days in this campaign, the relationship between nitrate formation pathways and pollution intensity warrants further investigation across seasons and contrasting meteorological conditions.”

(Lines 479–481) "[…] As these conclusions reflect processes observed during a one-week spring campaign, expanded measurements across multiple seasons and meteorological regimes would be needed to establish climatological representativeness. […]"

R2C3: In Methods, section 2.3.2, the inclusion and exclusion of certain pathways during daytime and nighttime analysis reads arbitrary. It is recommended to provide results of sensitivity tests for the mentioned inclusion and exclusion to see if such decisions alter the results or not in the SI.

Response: We thank the reviewer for the suggestion. To justify the selection of pathways for the nighttime nitrate formation analysis, we performed a sensitivity analysis comparing three different model configurations (C0–C2):

- C0 (original): $P_{RO_2\text{-}OH1}$, $P_{RO_2\text{-}het}$, and $P_{O_3\text{-}het}$
- C1 (full): $P_{RO_2\text{-}OH1}$, $P_{RO_2\text{-}OH2}$, $P_{RO_2\text{-}het}$, $P_{O_3\text{-}OH1}$, $P_{O_3\text{-}OH2}$, $P_{O_3\text{-}het}$
- C2 (nighttime only): $P_{RO_2\text{-}het}$ and $P_{O_3\text{-}het}$,

The results demonstrate that C0 provides the best fit. In addition, excluding P1a (C2) leads to a sharp increase in the absolute differentiation (averaged error) from 4.34‰ to 14‰, as these models fail to capture observed low $\delta^{18}O$ values (< 40‰). Furthermore, the full model (C1) did not improve accuracy (averaged error of 5.65‰) and introduced unnecessary complexity due to the identical ^{18}O signatures of $P_{RO_2\text{-}OH2}/P_{RO_2\text{-}het}$ and $P_{O_3\text{-}OH2}/P_{O_3\text{-}het}$. Consequently, C0 was selected as the optimized setting.

Sample ID	Measured $\delta^{18}O$ (‰)	Reconstructed $\delta^{18}O$ (‰) (absolute difference, ‰)		
		C0 (4.34)	C1 (5.65)	C2 (14)
17N	35.86	43.18 (7.32)	44.99 (9.13)	60.05 (24.19)
18N	33.81	42.71 (8.90)	44.54 (10.72)	59.99 (26.18)
19N	73.27	72.48 (0.79)	71.91 (1.36)	74.13 (0.86)
20N	31.94	42.42 (10.47)	44.03 (12.09)	59.97 (28.02)
21N	69.49	69.29 (0.20)	69.02 (0.47)	70.14 (0.65)
22N	43.37	46.01 (2.65)	48.26 (4.89)	60.30 (16.93)
23N	64.79	64.85 (0.06)	65.65 (0.86)	65.56 (1.17)

Contribution of each pathway in C0 (and C1):

Sample ID	Measured $\delta^{18}O$ (‰)	Fractional contribution					
		$P_{RO_2\text{-}OH1}$	$P_{RO_2\text{-}OH2}$	$P_{RO_2\text{-}het}$	$P_{O_3\text{-}OH1}$	$P_{O_3\text{-}OH2}$	$P_{O_3\text{-}het}$
17N	35.86	0.91(0.85)	(0.03)	0.06(0.04)	(0.04)	(0.02)	0.03(0.02)
18N	33.81	0.93(0.87)	(0.03)	0.05(0.03)	(0.03)	(0.02)	0.03(0.02)
19N	73.27	0.16(0.09)	(0.17)	0.27(0.14)	(0.14)	(0.23)	0.58(0.23)
20N	31.94	0.94(0.88)	(0.03)	0.04(0.03)	(0.03)	(0.02)	0.02(0.02)
21N	69.49	0.19(0.12)	(0.18)	0.33(0.16)	(0.16)	(0.19)	0.48(0.19)
22N	43.37	0.80(0.73)	(0.06)	0.14(0.07)	(0.07)	(0.03)	0.06(0.03)
23N	64.79	0.24(0.16)	(0.18)	0.41(0.19)	(0.20)	(0.13)	0.36(0.14)

This point was updated in section 2.3.2 of the revised manuscript (Lines 182−183) and in Description 3, Tables S3 and S4 of SI as follows:

(Lines 182−183) "[…] Sensitivity analyses regarding pathway exclusion are detailed in Supplementary Description S4, Tables S3 and S4."

"Description S4. Sensitivity analyses on the nitrate formation pathway

Sensitivity analyses were performed to compare three different model configurations (C0–C2):

- C0 (main text): $P_{RO_2\text{-}OH1}$, $P_{RO_2\text{-}het}$, and $P_{O_3\text{-}het}$
- C1 (full): $P_{RO_2\text{-}OH1}$, $P_{RO_2\text{-}OH2}$, $P_{RO_2\text{-}het}$, $P_{O_3\text{-}OH1}$, $P_{O_3\text{-}OH2}$, $P_{O_3\text{-}het}$
- C2 (nighttime only): $P_{RO_2\text{-}het}$ and $P_{O_3\text{-}het}$,

The results demonstrate that C0 provides the best fit. In addition, excluding P1a (C2) leads to a sharp increase in the absolute differentiation (averaged error) from 4.34‰ to 14‰, as these models fail to capture observed low $\delta^{18}O$ values (< 40‰) (Table S3). Furthermore, the full model (C1) did not improve accuracy (averaged error of 5.65‰) and introduced unnecessary complexity due to the identical ^{18}O signatures of $P_{RO_2\text{-}OH2}/P_{RO_2\text{-}het}$ and $P_{O_3\text{-}OH2}/P_{O_3\text{-}het}$ (Figure S4). Consequently, C0 was selected as the optimized setting."

Table S3. Reconstructed $\delta^{18}O$ (‰) from MixSIAR results of C0, C1, and C2 scenarios.

Sample ID	Measured $\delta^{18}O$ (‰)	Reconstructed $\delta^{18}O$ (‰) (absolute difference, ‰)		
		C0 (4.34)	C1 (5.65)	C2 (14)
17N	35.86	43.18 (7.32)	44.99 (9.13)	60.05 (24.19)
18N	33.81	42.71 (8.90)	44.54 (10.72)	59.99 (26.18)
19N	73.27	72.48 (0.79)	71.91 (1.36)	74.13 (0.86)
20N	31.94	42.42 (10.47)	44.03 (12.09)	59.97 (28.02)
21N	69.49	69.29 (0.20)	69.02 (0.47)	70.14 (0.65)
22N	43.37	46.01 (2.65)	48.26 (4.89)	60.30 (16.93)
23N	64.79	64.85 (0.06)	65.65 (0.86)	65.56 (1.17)

Table S4. Fractional contribution of each nitrate formation pathway in C0 (and C1).

Sample ID	Measured $\delta^{18}O$ (‰)	Fractional contribution of C0 (and C1)					
		$P_{RO_2\text{-}OH1}$	$P_{RO_2\text{-}OH2}$	$P_{RO_2\text{-}het}$	$P_{O_3\text{-}OH1}$	$P_{O_3\text{-}OH2}$	$P_{O_3\text{-}het}$
17N	35.86	0.91(0.85)	(0.03)	0.06(0.04)	(0.04)	(0.02)	0.03(0.02)
18N	33.81	0.93(0.87)	(0.03)	0.05(0.03)	(0.03)	(0.02)	0.03(0.02)
19N	73.27	0.16(0.09)	(0.17)	0.27(0.14)	(0.14)	(0.23)	0.58(0.23)
20N	31.94	0.94(0.88)	(0.03)	0.04(0.03)	(0.03)	(0.02)	0.02(0.02)
21N	69.49	0.19(0.12)	(0.18)	0.33(0.16)	(0.16)	(0.19)	0.48(0.19)
22N	43.37	0.80(0.73)	(0.06)	0.14(0.07)	(0.07)	(0.03)	0.06(0.03)
23N	64.79	0.24(0.16)	(0.18)	0.41(0.19)	(0.20)	(0.13)	0.36(0.14)

R2C4: In Results, Line 270-284 and Figure 4 are too speculative to me. I am not convinced how useful it is to have three independent linear regression lines on such limited data points. Moreover, grouping the clear data into <~1 micron and >1 micron reads arbitrary and is too mechanical. The hypotheses and suggested explanations were not supported by any ancillary or referable data, and I am not sure if the trend or differences are statistically significant. For

example, if the cutoff is not at 1 micron but at 1.5 or 2 micron, will the revealed increase go from 7.14 to 16.08 per mil? Will the $\delta^{15}N\text{-}NH_4^+$ values of this group really be lower then? When you say "coarse particles (1−10 μm) are likely produced from urban areas…that were subsequently transported to the sampling site", does your wind data support such a hypothesis? I agree that a bell-shaped pattern is revealed in Figure 4 and it becomes less apparent during the fog, but the corresponding discussions shall be revised with more supporting evidence.

Response: We thank the reviewer for the critical comment. We updated Figure 4 and the descriptions for Figure 4 in section 3.3.1 (Lines 264−293) of the revised manuscript as follows:

> (Lines 264−293) "Under clear conditions (excluding 19N and 21D), the size-resolved $\delta^{15}N\text{-}NH_4^+$ distribution revealed a bell-shaped distribution (Fig. 4). Values peaked at ~15‰ in the accumulation mode (~0.5−2 μm) and decreased to ~7‰ in both the ultrafine and coarse particles. This pattern reflects a transition between local emissions and aged, transported aerosols. For ultrafine mode (<0.5 μm), particles maintain isotopic equilibrium with the local NH_3 pool, dominated by $\delta^{15}N$-depleted residual NH_3 or volatilization sources (typically −28.3‰ to −17.6‰). For accumulation-mode (~0.5–2 μm), particles preserve the signatures of lower-elevation anthropogenic emission regions. Here, combustion-derived NH_3 (typically −8.2‰ to 1.8‰) reacts with H_2SO_4 to form non-volatile ammonium sulfate and ammonium bisulfate. Unlike ammonium nitrate, which is more volatile and easily re-equilibrates with gas-phase NH_3 during transport, sulfate-bound NH_4^+ is more resistant to isotopic re-equilibration, allowing it to act as a conservative tracer of urban source signatures during upslope transport (Wu et al., 2022). For the coarse mode (> 2 μm), particles are likely dominated by mineral dust and sea salt and present a substantially weaker thermodynamic sink for NH_3 absorption compared to acidic fine-mode sulfate aerosols (Fig. S6) (Pye et al., 2020). Therefore, NH_4^+ in this mode likely maintains a dynamic equilibrium with local gas-phase NH_3, which becomes progressively depleted in ^{15}N as the air mass ages.
>
> During fog, the bell-shaped distribution flattened significantly. Weakened wind suppressed the upslope transport of enriched anthropogenic pollutants, while enhanced aqueous-phase interaction promoted uniform isotopic re-equilibrium across all sizes. The high NO_3^- concentration from aqueous chemistry can also promote the local isotopically depleted NH_3 partitioning into the particle phase, dampening the size-dependent isotopic gradient.
>
> The flat $\delta^{15}N\text{-}NH_4^+$ size distribution was also observed on 19N and 21D. For 19N, it is likely a legacy effect of the preceding fog period (18D, 18N, and 19D). The NH_3 pool remained isotopically depleted from sustained fog-driven scavenging and re-equilibration, and regional transport had not yet replenished the accumulation-mode signal. However, high sub-micrometer NO_3^- concentration (Fig. S4) suggests that fog-like aqueous chemistry persisted, maintaining isotopic signatures similar to 18D. Conversely, the flat distribution on 21D reflects a distinct source influence. HYSPLIT back-trajectories (Fig. S7) indicate that the air parcel traveled through agricultural regions characterized by heavily depleted NH_3 (e.g., livestock waste, −28.3‰ to −17.6‰). The partitioning of this isotopically light NH_3 during transit effectively erased the characteristic accumulation-mode enrichment.

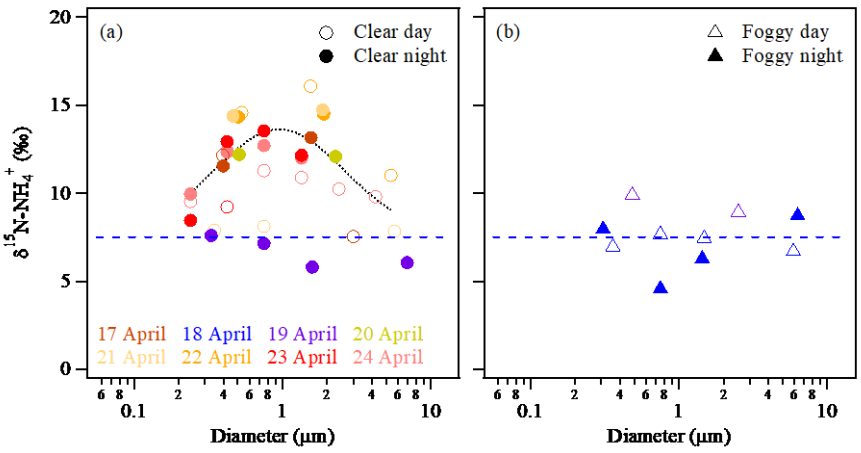

Figure 4. $\delta^{15}N$ of size-segregated pNH_4^+ during (a) clear and (b) foggy conditions. The dashed blue line indicates the mean $\delta^{15}N\text{-}NH_4^+$ for foggy periods. The dotted curve represents LogNormal distribution fits for clear conditions, excluding 19N and 21D, where no distinct bell-shaped size dependence was identified."

R2C5: Figures corresponding to results discussed in sections 3.4.2 and 3.4.3 are all in the SI. I'd suggest combining the two sections into one and bringing Figure S14 into the main manuscript for better interpretation. You may consider discussing the shifts in formation pathways (PXa, PXb) in a more descriptive, mechanistic language (Line 380 onward). I'd also suggest highlighting the importance of your pathway identifications (even though with uncertainties and assumptions) for improving the understanding of the particulate nitrate formation. Recent studies coupling the organonitrates formation during day and night with varied meteorological conditions, such as a few listed below, could be used for your reference and to put your findings into the broader picture:

Guo et al., 2024 (https://doi.org/10.1016/j.atmosenv.2024.120362)

Ward et al., 2025 (https://doi.org/10.1126/sciadv.adt8957)

Murphy et al., 2025 (https://doi.org/10.1021/acsestair.5c00206).

Response: We thank the reviewer for this suggestion. Sections 3.4.2 and 3.4.3 have been combined into a single section in the revised manuscript, and Figure S14 has been promoted to Figure 7. We have also updated the discussion of shifts in formation pathways and added two new paragraphs: one elaborating on the significance of pathway identification, and another addressing organon nitrate formation. This point was updated in the revised manuscript in section 3.4.2 (Lines 394−446) as follows:

> (Lines 394−446) "Formation pathways of pNO_3^- were quantitatively analyzed using the MixSIAR framework based on $\delta^{18}O\text{-}NO_3^-$ values, as shown in Fig. 7a. During daytime periods characterized by low $\delta^{18}O\text{-}NO_3^-$ values (31−41‰) and low CO concentrations (< 0.22ppm, 17D, 19D, and 23D), $P_{RO_2\text{-}OH1}$ accounted for 82−92% of pNO_3^- formation (Fig. 7a and 7b). These conditions are consistent with periods with limited influence from urban air masses, suggesting the dominance of local RO_2 oxidation processes. In contrast, during daytime with higher $\delta^{18}O\text{-}NO_3^-$ values (63−70‰) and to elevated CO

concentrations (0.24−0.27 ppm, 18D, 21D, 22D), the dominant pathways shifted toward $P_{RO_2\text{-}OH2}$, $P_{O_3\text{-}OH1}$, and $P_{O_3\text{-}OH2}$, contributing an average of 29±1%, 27±3%, and 28±5%, respectively. This shift could probably reflect the enhanced transport of urban air masses enriched in O_3 and NO_x precursors.

Although nighttime nitrate formation is theoretically dominated by heterogeneous reactions, our results reveal a more complex process. On nights with elevated $\delta^{18}O\text{-}NO_3^-$ values, heterogeneous pathways ($P_{RO_2\text{-}het}$ and $P_{O_3\text{-}het}$) were the dominant contributors, accounting for 33±6% and 47±9% of pNO_3^- formation on 19N, 21N, 23N. In contrast, on nights with lower $\delta^{18}O\text{-}NO_3^-$ values (32−43‰, 17N, 18N, 20N, and 22N), $P_{RO_2\text{-}OH1}$ remained a major contributor, accounting for 80−94% of formation. This high $P_{RO_2\text{-}OH1}$ might stem from the residual pNO_3^- from daytime, or nighttime ·OH generated via reactions between O_3 and alkenes/terpenes (Kroll et al., 2001; Aschmann et al., 2002). The weak night-to-night covariation between $\delta^{18}O\text{-}NO_3^-$ and CO concentrations further suggests that nighttime nitrate isotope signatures are governed by the interplay among fog processing, reduced advection, and heterogeneous chemistry, rather than transport intensity alone.

A distinct shift in nitrate formation pathways was observed during the fog. On 18D, high $\delta^{18}O\text{-}NO_3^-$ values (70‰) and elevated CO concentrations (0.24 ppm) were associated with the dominance of $P_{RO_2\text{-}OH2}$ (30±20%) and $P_{O_3\text{-}OH2}$ (36±16%), indicating that O_3 from transported urban precursors remained active (Fig. S15). As fog intensified during 18N and persisted into 19D, $\delta^{18}O\text{-}NO_3^-$ values decreased sharply to ~34‰, and $P_{RO_2\text{-}OH1}$ became dominant (93±5% on 18N, and 90±5% on 19D). This transition is driven by two coupled effects: (1) the attenuation of incoming solar radiation suppresses O_3 photolysis and thereby reduces the availability of high-$\delta^{18}O$ oxidants, and (2) the scavenging of long-range transport by wet deposition diminishes the influx of urban NO_x and O_3. Together, these foggy conditions favor locally derived low-$\delta^{18}O$ RO_2 cycling as the predominant oxidant driving nitrate formation.

Distinguishing the relative contributions helps clarify how nitrate formation processes vary with air mass origin, photochemical activity, and fog processing, which is directly relevant to emission control strategies since the efficacy of nitrate reduction depends on the dominant oxidation pathway. At the global scale, model estimated that the NO_2 + ·OH (same as our $P_{O_3\text{-}OH1}/P_{O_3\text{-}OH2}$) and N_2O_5 hydrolysis (same as our $P_{RO_2\text{-}het}/P_{O_3\text{-}het}$) pathways each contributed approximately 41% to tropospheric nitrate formation (Alexander et al., 2020), while observation studies in both urban and mountain environments suggest that heterogeneous pathways become more important for nitrate formation under elevated pollution levels (Fan et al., 2020; Lin et al., 2021). The pathway apportionment presented here provides finer resolution than bulk gas-phase/heterogeneous partitioning by explicitly distinguishing RO_2- from O_3-initiated formation, which can be useful in regions where RO_2 oxidation dominates. However, given the limited number of sampling days in this campaign, the relationship between nitrate formation pathways and pollution intensity warrants further investigation across seasons and contrasting meteorological conditions.

Beyond inorganic HNO_3 formation, the total particulate nitrogen budget includes particulate organic nitrate (pON) species, which can account for 17−31% of total

particulate nitrogen (Yu et al., 2024) in mixed urban-biogenic environments, and up to 50% observed in urban plumes (Murphy et al., 2025). *p*ON forms via the reaction of NO with RO_2 (NO + RO_2 → $RONO_2$) during the day, and NO_3 with alkenes and biogenic VOC at night (NO_3 + R → $RONO_2$) (Murphy et al., 2025; Ward et al., 2025; Guo et al., 2024). These mechanisms operate through the same RO_2- and NO_3-driven pathways identified here ($P_{RO_2\text{-}OH1}$ / $P_{RO_2\text{-}OH2}$ and $P_{RO_2\text{-}het}$/$P_{O_3\text{-}het}$, respectively), suggesting that the oxidation chemistry inferred from $\delta^{18}O\text{-}NO_3^-$ signatures at Xitou also drives concurrent *p*ON production. Because isotope analysis in this study assumes TN comprises only NO_3^- and NH_4^+, organic nitrogen contribution could bias the derived $\delta^{15}N\text{-}NH_4^+$ toward the signature of *p*ON. While this was partially mitigated by excluding samples with low $[NH_4^+]$ (<60% of ([TN]−[NN])), future research should prioritize direct $\delta^{15}N\text{-}NH_4^+$ measurement, which would enable the estimation of organic nitrate isotopes via residual mass balance (i.e., [ON] = [TN] – $[NH_4^+]$ – $[NO_3^-]$) and provide a more complete characterization of the Nr budget in mountain forest environments.

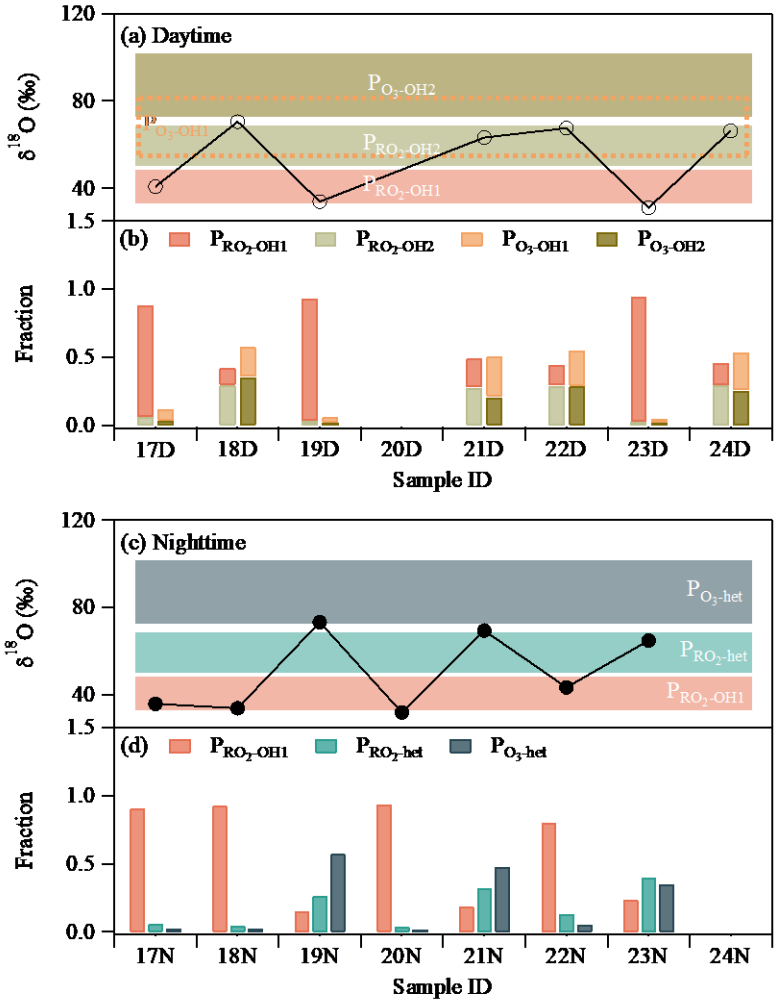

Figure 7. Contributions of nitrate formation pathways estimated by MixSIAR. (a, c) Measured $\delta^{18}O\text{-}NO_3^-$ values with the corresponding $\delta^{18}O$ ranges of potential formation pathways. (b, d) estimated fractional contributions of these pathways.”

Technical corrections:

R2C6: In Figure 6a, I am not sure if the regression line is needed given how scattered the data are.

Response: We have removed the regression line in Figure 6a in the revised manuscript to avoid over-interpreting the relationship between these variables.

R2C7: Same as above for Figure S15.

Response: The regression line in Figure S15 has also been removed in the revised manuscript.

R2C8: What's your take on larger particles being more neutral and smaller being more acidic from your Figure S6? Is it consistent with your hypothesis that more coarse particles were transported from the urban area?

Response: We thank the reviewer for this comment. Figure S6 is based on FTIR-derived ionic concentrations, which show a size-dependent acidity gradient with finer particles appearing more acidic and coarser particles more neutral. However, we note that IC-based measurements, which provide more quantitatively reliable ionic concentrations, do not show a clear systematic acidity gradient across size fractions (Fig. S6 in the revised manuscript). Given the known limitations of FTIR for quantitative ion concentration retrieval compared to IC, we consider the IC-based assessment more robust for evaluating particle neutralization state. In the IC-based data (Fig. S6), fine particles are approximately charge-balanced, while coarse particles exhibit an apparent anion excess, likely attributable to unmeasured crustal or sea-salt cations (e.g., Na^+, Ca^{2+}, Mg^{2+}) which were not quantified in this study. We've updated Figure S6 and the description about this part in section 3.3.1 (Lines 264–277) of the revised manuscript as follows:

(Figure S6)

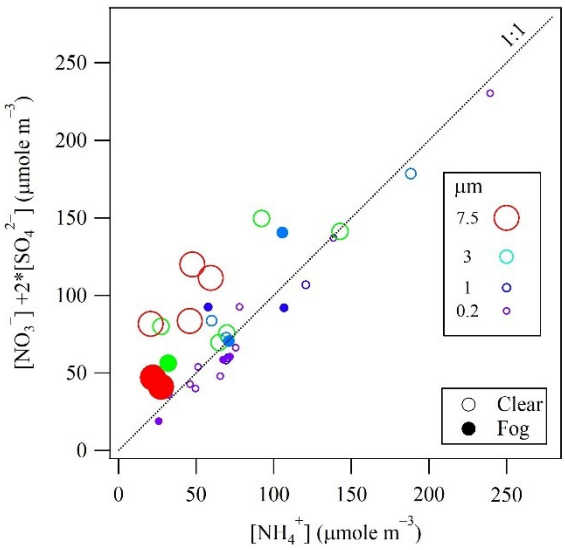

Figure S6. Scatter plot of $[NO_3^-] + 2*[SO_4^{2-}]$ versus $[NH_4^+]$ measured by ion chromatography during the observation period.

(Lines 264–277) "Under clear conditions (excluding 19N and 21D), the size-resolved $\delta^{15}N\text{-}NH_4^+$ distribution revealed a bell-shaped distribution (Fig. 4). Values peaked at ~15‰ in the accumulation mode (~0.5–2 μm) and decreased to ~7‰ in both the ultrafine and coarse particles. This pattern reflects a transition between local emissions and aged, transported aerosols. For ultrafine mode (<0.5 μm), particles maintain isotopic equilibrium with the local NH_3 pool, dominated by $\delta^{15}N$-depleted residual NH_3 or volatilization sources (typically −28.3‰ to −17.6‰). For accumulation-mode (~0.5–2 μm), particles preserve the signatures of lower-elevation anthropogenic emission regions. Here, combustion-derived NH_3 (typically −8.2‰ to 1.8‰) reacts with H_2SO_4 to form non-volatile ammonium sulfate and ammonium bisulfate. Unlike ammonium nitrate, which is more volatile and easily re-equilibrates with gas-phase NH_3 during transport, sulfate-bound NH_4^+ is more resistant to isotopic re-equilibration, allowing it to act as a conservative tracer of urban source signatures during upslope transport (Wu et al., 2022). For the coarse mode (> 2 μm), particles are likely dominated by mineral dust and sea salt and present a substantially weaker thermodynamic sink for NH_3 absorption compared to acidic fine-mode sulfate aerosols (Fig. S6) (Pye et al., 2020). Therefore, NH_4^+ in this mode likely maintains a dynamic equilibrium with local gas-phase NH_3, which becomes progressively depleted in ^{15}N as the air mass ages."

References

Alexander, B., Sherwen, T., Holmes, C. D., Fisher, J. A., Chen, Q., Evans, M. J., and Kasibhatla, P.: Global inorganic nitrate production mechanisms: comparison of a global model with nitrate isotope observations, Atmos. Chem. Phys., 20, 3859-3877, https://doi.org/10.5194/acp-20-3859-2020, 2020.

Aschmann, S. M., Arey, J., and Atkinson, R.: OH radical formation from the gas-phase reactions of O_3 with a series of terpenes, Atmos. Environ., 36, 4347-4355, https://doi.org/10.1016/S1352-2310(02)00355-2, 2002.

Chen, C.-L., Chen, T.-Y., Hung, H.-M., Tsai, P.-W., Chou, C. C. K., and Chen, W.-N.: The influence of upslope fog on hygroscopicity and chemical composition of aerosols at a forest site in Taiwan, Atmos. Environ., 246, 118150, https://doi.org/10.1016/j.atmosenv.2020.118150, 2021.

Ervens, B.: Modeling the processing of aerosol and trace gases in clouds and fogs, Chem. Rev., 115, 4157-4198, https://doi.org/10.1021/cr5005887, 2015.

Fan, M.-Y., Zhang, Y.-L., Lin, Y.-C., Cao, F., Zhao, Z.-Y., Sun, Y., Qiu, Y., Fu, P., and Wang, Y.: Changes of emission sources to nitrate aerosols in Beijing after the clean air actions: Evidence from dual isotope compositions, J. Geophys. Res.: Atmos., 125, e2019JD031998, https://doi.org/10.1029/2019JD031998, 2020.

Guo, F., Bui, A. A. T., Schulze, B. C., Dai, Q., Yoon, S., Shrestha, S., Wallace, H. W., Sanchez, N. P., Alvarez, S., Erickson, M. H., Sheesley, R. J., Usenko, S., Flynn, J., and Griffin, R. J.: Airmass history, night-time particulate organonitrates, and meteorology impact urban SOA formation rate, Atmos. Environ., 322, 120362, https://doi.org/10.1016/j.atmosenv.2024.120362, 2024.

Kroll, J. H., Clarke, J. S., Donahue, N. M., Anderson, J. G., and Demerjian, K. L.: Mechanism of HO_x formation in the gas-phase ozone−alkene reaction. 1. Direct, pressure-dependent measurements of prompt OH yields, J. Phys. Chem. A, 105, 1554-1560, https://doi.org/10.1021/jp002121r, 2001.

Liang, Y.-L., Lin, T.-C., Hwong, J.-L., Lin, N.-H., and Wang, C.-P.: Fog and Precipitation Chemistry at a Mid-land Forest in Central Taiwan, J. Environ. Qual., 38, 627-636, https://doi.org/10.2134/jeq2007.0410, 2009.

Lin, Y.-C., Zhang, Y.-L., Yu, M., Fan, M.-Y., Xie, F., Zhang, W.-Q., Wu, G., Cong, Z., and Michalski, G.: Formation mechanisms and source apportionments of airborne nitrate aerosols at a Himalayan-Tibetan Plateau site: Insights from nitrogen and oxygen isotopic compositions, Environ. Sci. Technol., 55, 12261-12271, https://doi.org/10.1021/acs.est.1c03957, 2021.

Lin, Z., Ji, X., Xu, L., Chen, G., Yang, C., Zhang, K., Zhang, F., Li, L., Chen, Y., and Chen, J.: Enhanced NO_2-driven multiphase formation of particulate nitrate and sulfate under high-humidity conditions, npj Clim. Atmos. Sci., 9, 76, https://doi.org/10.1038/s41612-026-01352-5, 2026.

Murphy, S. E., Buenconsejo, R. S., Draper, D. C., Crounse, J. D., Baliaka, H. D., Ward, R. X., Schulze, B. C., Rezgui, S. P., Ball, K., Susskind, T., Kappaganthula, G., and Wennberg, P. O.: Multi-functional organic nitrogen in the Los Angeles Air Basin, ACS ES&T Air, 2, 2009-2027, https://doi.org/10.1021/acsestair.5c00206, 2025.

Pye, H. O. T., Nenes, A., Alexander, B., Ault, A. P., Barth, M. C., Clegg, S. L., Collett Jr, J. L., Fahey, K. M., Hennigan, C. J., Herrmann, H., Kanakidou, M., Kelly, J. T., Ku, I. T., McNeill, V. F., Riemer, N., Schaefer, T., Shi, G., Tilgner, A., Walker, J. T., Wang, T., Weber, R., Xing, J., Zaveri, R. A., and Zuend, A.: The acidity of atmospheric particles and clouds, Atmos. Chem. Phys., 20, 4809-4888, https://doi.org/10.5194/acp-20-4809-2020, 2020.

Ward, R. X., Baliaka, H. D., Schulze, B. C., Kerr, G. H., Crounse, J. D., Hasheminassab, S., Bahreini, R., Dillner, A. M., Russell, A., Ng, N. L., Wennberg, P. O., Flagan, R. C., and Seinfeld, J. H.: Poorly quantified trends in ammonium nitrate remain critical to understand future urban aerosol control strategies, Science Advances, 11, eadt8957, https://doi.org/10.1126/sciadv.adt8957, 2025.

Wey, T.-H., Lai, Y.-J., Chang, C.-S., Shen, C.-W., Hong, C.-Y., Wang, Y.-N., and Chen, M.-C.: Preliminary Studies on Fog Characteristics at Xitou Region of Central Taiwan, Jour. Exp. For. Nat. Taiwan Univ., 25, 149-160, https://doi.org/10.6542/EFNTU.201106_25(2).0006, 2011.

Wu, C., Cao, C., Li, J., Lv, S., Li, J., Liu, X., Zhang, S., Liu, S., Zhang, F., Meng, J., and Wang, G.: Different physicochemical behaviors of nitrate and ammonium during transport: a case study on Mt. Hua, China, Atmos. Chem. Phys., 22, 15621-15635, https://doi.org/10.5194/acp-22-15621-2022, 2022.

Xu, W., Kuang, Y., Xu, W., Liu, L., Xu, H., Wang, X., Liu, Y., Cheng, H., Zhang, X., Zhai, M., Liu, C., Liang, L., Zhang, G., Luo, B., Tao, J., Liu, J., Zhao, H., Ren, S., Zhou, G., Liu, P., Xu, X., and Sun, Y.: Efficient nitrate formation in fog events implicates fog interstitial aerosols as

significant drivers of atmospheric chemistry, Environ. Sci. Technol., 58, 22298-22311, https://doi.org/10.1021/acs.est.4c09078, 2024.

Yu, H.-R., Zhang, Y.-L., Cao, F., Zhao, Z.-Y., Fan, M.-Y., and Yang, X.-Y.: Fog event is possibly a source rather than a sink of atmospheric nitrate aerosols: Insights from isotopic measurements in Nanjing, China, Appl. Geochem., 155, 105721, https://doi.org/10.1016/j.apgeochem.2023.105721, 2023.

Yu, X., Li, Q., Liao, K., Li, Y., Wang, X., Zhou, Y., Liang, Y., and Yu, J. Z.: New measurements reveal a large contribution of nitrogenous molecules to ambient organic aerosol, npj Clim. Atmos. Sci., 7, 72, https://doi.org/10.1038/s41612-024-00620-6, 2024.

Zhang, G., Hu, X., Sun, W., Yang, Y., Guo, Z., Fu, Y., Wang, H., Zhou, S., Li, L., Tang, M., Shi, Z., Chen, D., Bi, X., and Wang, X.: A comprehensive study about the in-cloud processing of nitrate through coupled measurements of individual cloud residuals and cloud water, Atmos. Chem. Phys., 22, 9571-9582, https://doi.org/10.5194/acp-22-9571-2022, 2022.